



1 **Process-based modeling framework for sustainable irrigation**
2 **management at the regional scale: Integrating rice production, water**
3 **use, and greenhouse gas emissions**

4
5 Yan Bo^{1,6}, Hao Liang^{2,6}, Tao Li³, Feng Zhou^{2,4,5,*}

6
7 ¹ Institute of Carbon Neutrality, Laboratory for Earth Surface Processes, College of
8 Urban and Environmental Sciences, Peking University, Beijing, China.

9 ² National Key Laboratory of Water Disaster Prevention, Key Laboratory of Water
10 and Soil Processes in Watershed, College of Geography and Remote Sensing, Hohai
11 University, Nanjing, China

12 ³ International Rice Research Institute (IRRI), Los Baños, Philippines

13 ⁴ College of Urban and Environmental Sciences, Peking University, Beijing, China

14 ⁵ Southwest United Graduate School, Kunming, China

15 ⁶ These authors contributed equally

16

17 * *Correspondence to:* Feng Zhou (zhouf@pku.edu.cn)



18 **Abstract**

19 Rice cultivation faces multiple challenges of rising food demand while increasing water
20 scarcity and greenhouse gas emissions, intensifying the tension of the food-water-
21 climate nexus. Process-based modeling of the nexus is pivotal for developing effective
22 measures to address these challenges. However, current models struggle to simulate
23 their complex relationships under different water management schemes, primarily due
24 to inadequate representation of critical physiological effects and the absence of efficient
25 spatially explicit modeling strategies. Here, we propose an advancing framework that
26 addresses these problems by integrating a process-based soil-crop model with vital
27 physiological effects, a novel method for model upscaling, and the NSGA-II multi-
28 objective optimization algorithm at a parallel computing platform. Applying the
29 framework accounted for 52%, 60%, 37%, and 94% of the experimentally observed
30 variations in rice yield, irrigation water use, and methane and nitrous oxide emissions
31 in response to irrigation schemes. Compared with the origin model using traditional
32 parameter upscaling methods, the advancing framework significantly reduced
33 simulation errors by 35%–85%. Moreover, it well reproduced the multivariable
34 synergies and tradeoffs observed in China’s rice fields and identified additional 18%
35 areas feasible for irrigation optimization, along with an additional 11% and 14%
36 reduction potentials of water use and methane emissions, without compromising
37 production. Over 90% of the potentials could be realized at the cost of 4% less yield
38 increase and 25% higher nitrous oxide emissions under multiple objectives. Overall,
39 this study provides a valuable tool for multi-objective optimization of rice irrigation
40 schemes. The advancing framework also has implications for other process-based
41 modelling improvements efforts.

42
43 **Key points**

- 44 ● This study significantly improved rice yield simulations under various irrigation
45 schemes by quantifying and incorporating critical physiological processes into a
46 process-based model.
- 47 ● This study developed a novel upscaling method of model parameterization that
48 well reproduced observed synergies and tradeoffs among multiple objectives (i.e.,
49 rice yield, irrigation water use, methane emissions, and nitrous oxide emissions).
- 50 ● This study provides a practical tool for multi-objective optimization of water
51 management to deliver co-benefits of ensuring food production, saving water, and
52 reducing greenhouse gas emissions of rice fields.



53

54 **1 Introduction**

55

56 Rice is the staple food for more than half of the world's population and is also the most
57 water-intensive cereal crop with a significant contribution to greenhouse gas emissions
58 (GHGs) (Lampayan et al., 2015; Carlson et al., 2017). Rice cultivation currently
59 accounts for 40% of global irrigation water use (IRR), 30% of methane (CH₄), and 11%
60 of nitrous oxide (N₂O) emissions in agriculture (Yuan et al., 2021). To meet the demand
61 of the growing population, a 50-60% increase in global rice production along with a
62 15% increase in water use are required by 2050, potentially leading to higher
63 greenhouse gas emissions and intensifying the food-water-climate tensions of rice
64 fields (Flörke et al., 2018). Therefore, ensuring food security while conserving water
65 resources and reducing GHGs in rice cultivation is essential for achieving multiple
66 United Nations Sustainable Development Goals.

67

68 Optimizing water management is promising to address the multiple challenges.
69 However, different water management schemes can lead to a wide range of outcomes
70 in rice yield (−16.9% to 21.9%), IRR (−68.0% to −0.3%), CH₄ (−85.5% to −0.1%) and
71 N₂O (0% to 364%) across climatic zones, reflecting complex interactions between
72 environmental factors and management strategies (Bo et al., 2022). Process-based
73 models are powerful tools for predicting and managing the complicated interactions in
74 responses to water management, given their strength in simulating crop growth, water
75 dynamics, and soil biogeochemical processes under diverse genotype × environment ×
76 management conditions (Tian et al., 2021; Chen et al., 2022; Yan et al., 2024). Despite
77 with several relevant studies at site-scales, extrapolation of optimized water
78 management schemes from limited sites to the broader rice growing regions is hindered
79 by the diverse climate, soil, crop variety, field management, etc. (Yan et al., 2024; Liang
80 et al., 2021). Region-specific simulations of the food-water-climate nexus are thus
81 urgently needed to identify tailored solutions. Nevertheless, current models face
82 challenges in accurately predicting yield responses to various water management
83 practices and adequately reproducing the spatial heterogeneity of these responses.

84

85 Despite extensive experimental research to understand critical physiological effects
86 underlying yield responses, these processes have not been fully represented in models,
87 especially the compensation mechanisms. Compared to continuous flooding, imposing
88 moderate water deficit and then rewatering the field could increase both effective leaf
89 area and net photosynthetic rate upon re-irrigation to enhance photosynthesis for
90 biomass production (Yang and Zhang, 2010). In addition, harvest index could increase
91 due to enhanced remobilization of assimilates and accelerated grain filling rate (Zhang
92 et al., 2008). However, prevailing models (for example, ORYZA, DSSAT, APSIM,
93 WHCNS) primarily focus on the negative impacts of water deficit (i.e., reduced
94 photosynthesis or leaf rolling), while neglecting or indirectly simulating crop
95 adaptation processes (e.g., enhanced root growth and water uptake in deeper soil layers)
96 (Bouman et al., 2001; Li et al., 2017; Liang et al., 2021; Tsuji et al., 1998). As a



97 consequence, yield sensitivities to water management could be overestimated, as
98 evidenced by evaluations of the ORYZA (v3) model (Xu et al., 2018). Moreover,
99 physiological processes respond differently to water availability at different growth
100 stages, while crop models generally use constant water effect coefficient throughout the
101 rice growing season (Ishfaq et al., 2020). These imply model deficiencies in predicting
102 yield response to water management, although no assessment across large scales exists.

103
104 Accurate model parameters are essential for reproducing spatial heterogeneity of yield,
105 IRR, and GHGs. Previous studies usually used either the same parameters at different
106 pixels, calibrated against all observations, or the spatial proximity principle to
107 extrapolate model parameters for regional simulations, as a result of lacking enough
108 observations (Zhang et al., 2024; Zhang et al., 2016). However, critical model
109 parameters varied considerably when calibrated under different environmental and
110 management conditions, reflecting important impact of these factors on underlying
111 physiological and biogeochemical processes (Tan et al., 2021). As a consequence,
112 traditional model parameterization approaches are unlikely to capture variability of
113 yield, IRR, and GHGs due to their neglect of the environmental and management-
114 related impacts (Song et al., 2023; Zhang et al., 2023). Besides, previous studies only
115 evaluated simplified irrigation protocols (i.e., once drainage at midseason or alternative
116 wetting and drying with constant threshold across the growing season) or only set bi-
117 objectives as optimization targets (Tian et al., 2021; Chen et al., 2022), which likely
118 underestimated the regulation potentials. Therefore, an integrated framework composed
119 of a reliable modelling platform, broader water management schemes and multi-
120 objective optimization targets are required for sustainable water management
121 optimization.

122
123 To address these challenges, this study proposed an advancing framework that
124 integrated a process-based soil-crop model (Soil Water Heat Carbon Nitrogen Simulator,
125 WHCNS) with key physiological effects, a novel model upscaling method, and the
126 NSGA-II multi-objective optimization algorithm at a parallel computing platform (see
127 Fig.1 for workflow). This study focused on rice yield (Yield), irrigation water use (IRR),
128 methane (CH₄), and nitrous oxide emissions (N₂O) of irrigated rice fields. First, three
129 physiological effects were quantified and embedded into WHCNS to enhance the
130 prediction of yield responses. Regionalized model parameters were then derived by
131 developing parameter transfer functions for regional simulations. The model's ability
132 to reproduce the variations in the food-water-climate nexus was extensively validated
133 against field observations. Multi-objective optimization was conducted using the
134 NSGA-II algorithm to investigate tradeoffs within the food-water-climate nexus and
135 assess the regulation potentials of water management optimization. This framework
136 was applied to China's rice cropping system as an example, considering its position as
137 the world's largest rice producer and the ongoing conflicts between production demand,
138 water scarcity, and greenhouse gas emissions. This study aims to provide a valuable
139 framework for predicting and regulating rice's food-water-climate nexus towards
140 sustainable water management.



141

142 **2 Data and Methods**

143 **2.1 WHCNS model and input data**

144

145 The soil Water Heat Carbon Nitrogen Simulator (WHCNS) model was improved and
146 incorporated into the advancing framework in this study to simulate rice yield, irrigation
147 water use (IRR), methane (CH₄), and nitrous oxide (N₂O) emissions of irrigated rice
148 fields at each pixel. The WHCNS model is a process-based agroecosystem model that
149 runs at a daily time step and comprises six major components: surface ponding water
150 dynamic, soil water movements, soil heat transfer, soil N transformation and transport,
151 soil organic turnover, and crop growth. Detailed model descriptions can be found in
152 (Liang et al., 2022; Liang et al., 2023; Liang et al., 2021). This model was chosen for
153 several considerations: (i) the model directly outputs all four target variables
154 simultaneously. This avoids biogeochemical models relying on crop models for detailed
155 physiological parameters to simulate yield and calculating IRR externally to obtain all
156 four targets as previously done (Tian et al., 2021; Yan et al., 2024), (ii) the model has
157 been proven to simulate frequent dry-wet cycles effect reasonably well in China rice
158 fields, due to simulating water and nitrogen dynamics in surfacing ponding water layer
159 that is specific for rice fields (Liang et al., 2021), (iii) the model is executable at both
160 site and regional scales with high efficiency and performs well in capturing spatial
161 variation in key processes (Liang et al., 2023), (iv) the model has a very flexible
162 irrigation setup, which allows for the precise control of paddy field water surface levels
163 by setting the minimum and maximum irrigation thresholds. It also enables calculating
164 water usage for paddy field irrigation under various water management scenarios (Jiang
165 et al., 2021). The model is particularly suitable for simulating the regional food-water-
166 climate nexus of rice fields.

167

168 This study ran the model at both site and regional scales (0.5-degree spatial resolution).
169 Model input data includes daily meteorological variables, soil properties by depth, and
170 management variables related to planting, fertilization, and irrigation. For site-scale
171 simulations, these variables were obtained from experimental studies, if unreported,
172 were extracted from spatial datasets according to geographical locations. All spatial
173 datasets were all resampled to 0.5-degree spatial resolution for regional simulations. (1)
174 Meteorological variables, including daily mean, maximum and minimum air
175 temperature, wind speed, precipitation, humidity, and downward solar radiation, were
176 obtained from the fifth generation ECMWF reanalysis (ERA5) at 0.25-degree
177 resolution (Hersbach et al., 2018) . (2) Soil data including bulk density, clay contents,
178 and soil hydraulic properties (i.e., saturated water content, field water capacity, wilting
179 point, saturated hydraulic conductivity) at soil depths of 5, 15, 30, 60, 100, and 200 cm
180 was obtained from SoilGrids (10 km) (Han et al., 2015) . (3) The planting and harvest
181 dates were obtained from the crop calendar data of Global Gridded Crop Model
182 Intercomparisons (GGCMI) Phase 3 (Jägermeyr et al., 2021). (4) Fertilization practices
183 were conducted by the auto-fertilization component of the WHCNS model, assuming
184 no nitrogen stress (Liang et al., 2023). (5) Irrigation practices are defined by three



185 variables at daily step, including upper threshold (U_{IRR}), lower threshold (L_{IRR} , with a
186 positive value representing field water level and a negative value representing soil water
187 potential at 15 cm below the soil surface) and maximum allowable field water level
188 after rainfall (H_p , also refers to as bund height). Since there is no spatially explicit
189 information about realistic water management schemes, daily irrigation thresholds were
190 set following [Chen et al. \(2022\)](#) for regional simulations. The model simulates field
191 water level of surface ponding layer and soil water potential of stratified layers at daily
192 step. Irrigation would be triggered whenever field water level ($L_{IRR} > 0$) or soil water
193 potential at 15 cm below the soil surface ($L_{IRR} < 0$) reach the predetermined L_{IRR} .
194 Irrigation demand is then calculated as the differences between L_{IRR} and U_{IRR} .

195

196 **2.2 Compilation of experimental observations**

197

198 Extensive literature reviews were conducted to collect experimental observations for
199 model improvement and parameters calibration. Relevant studies should meet the
200 following criteria: (1) only field experiments covering an entire growing season were
201 included, while pot and laboratory experiments under controlled environmental
202 conditions were excluded, (2) the control and treatments only differed concerning water
203 management with continuous flooding (CF) as control and non-continuous flooding
204 irrigation (NCF) as treatment, but not concerning other agronomic practices (e.g.,
205 cropping intensity, fertilizer management, and tillage). This was to isolate water
206 management effects while avoiding confounding effects of other factors, (3) upper and
207 lower irrigation thresholds were explicitly reported, and lower thresholds were
208 indicated by soil water potential measured at the soil depth of 15-20 cm. Observations
209 based on soil water potential at the other soil depth or the other soil-water indicators
210 (e.g., soil water contents) were excluded, (4) at least one of target variables were
211 observed, including rice yield (*Yield*), irrigation water use (*IRR*), methane emissions
212 (CH_4), nitrous oxide emissions (N_2O), leaf area index (*LAI*), net photosynthetic rate
213 (*Pn*), and harvest index (*HI*). For *LAI* and *Pn*, the growth stages of observations (i.e.,
214 tillering, booting, heading, and ripening stage) were recorded to account for growth
215 stage-dependent effects. As a result, we collected observations of 119 experiments from
216 37 studies covering 29 sites in 6 countries (i.e., China, India, Philippines, Japan,
217 Bangladesh, and Peru). These observations were split into two datasets according to
218 target variables. The first dataset including *Yield*, *IRR*, CH_4 , or N_2O observations was
219 used for calibration of model parameters. The second dataset of *LAI*, *Pn*, or *HI*
220 observations was used to quantify water management effects on physiological
221 processes for model improvement (Section 2.3).

222

223 For each paired observation under the control and treatment, the effects of non-
224 continuous flooding irrigation were calculated as the ratio of observations under
225 treatment to that under control (Equation 1). This yielded 251 records for R^{Yield} , 235 for
226 R^{IRR} , 37 for R^{CH_4} , 14 for R^{N_2O} , 561 for R^{LAI} (including 61 from tillering stage, 159 from
227 booting stage, 202 from heading stage and 139 from ripening stage), 84 for R^{Pn}
228 (including 42 from tillering stage, and 42 from filling stage), and 351 for R^{HI} .



229

230

$$R^X = \frac{X_{NCF}}{X_{CF}} \quad (1)$$

231 where R^X represents non-continuous flooding effects (NCF) on target variables X
232 (including $Yield$, IRR , CH_4 , N_2O , LAI , Pn , and HI), X_{NCF} and X_{CF} represent variable
233 values under non-continuous flooding (NCF) and continuous-flooding irrigation (CF),
234 respectively. Relative changes of target variables were calculated as $(R^X-1) \times 100$ for
235 interpretation and representation (e.g., $\Delta Yield$, ΔIRR , ΔCH_4 , ΔN_2O).

236

237 For each paired observation, four categories of information were also collected. First,
238 climatic variables included mean daily air temperature (T), precipitation (P), and crop
239 evapotranspiration (PET_c) during growing season. The difference between P and PET_c
240 was further calculated to indicate climatological water availability (CWA). Second, soil
241 variables included sand content, bulk density (BD), soil organic carbon (SOC), pH, and
242 soil hydrological properties (e.g., saturated water content (SAT), field water capacity
243 (FWC)). Third, management-related variables included nitrogen application rate and
244 timing, as well as lower (L_{AWD}) and upper (U_{AWD}) irrigation thresholds. Fourth,
245 experimental parameters included geographical location (latitude, longitude), dates of
246 seeding (also transplanting date in transplanted systems), anthesis, and harvest. These
247 variables were used for running WHCNS (Section 2.1) and conducting correlation
248 analyses (Section 3.1).

249

250 2.3 Model improvement

251 2.3.1 Incorporation of physiological effects

252

253 In the original WHCNS model, water management effects on crop growth were
254 simulated by calculating water stress factor based on the Feddes reduction function
255 (Feddes and Zaradny, 1978). Specifically, the water stress factor is calculated at daily
256 step as a function of soil water potential to reduce root water uptake, assuming 70 kpa
257 and 1500 kpa as thresholds of when root water uptake starts to decrease and approaches
258 0 (Equation 2-3). The calculated water stress factor was used to reduce the simulated
259 actual biomass production rate, which further indirectly impact produced biomass
260 allocated for leaf growth and yield formation (Equation 4-6).

261

$$T_a = \int_{L_R} S(h, h_\Phi, z) dz = T_p \int_{L_R} a_w(h, z) a_s(h_\Phi, z) b(z) dz \quad (2)$$



$$cf(w) = \frac{T_a}{T_p} = \begin{cases} \frac{\int_{L_R} a_w(h, z) a_s(h_\phi, z) b(z) dz}{\omega} = \frac{\omega}{\omega} = 1 & \omega > \omega_c \\ \frac{\int_{L_R} a_w(h, z) a_s(h_\phi, z) b(z) dz}{\omega_c} = \frac{\omega}{\omega_c} < 1 & \omega \leq \omega_c \end{cases} \quad (3)$$

$$Fgc = DL \times \frac{AMAX}{K_e} \times \ln \left[\frac{AMAX + CC}{AMAX + CC \times (-LAI \times K_e)} \right] \quad (4)$$

$$Fgass = Fgc \times \frac{30}{44} \times cf(w) \times cf(N) \quad (5)$$

266

$$GAA(org) = Fgass \times fr(org) \quad (6)$$

268

269 where T_a and T_p are actual and potential root water uptake (cm d^{-1}). L_R indicates root
270 length (cm). $a_w(h, z)$ and $a_s(h_\phi, z)$ are water and salt stress functions. $b(z)$ is root
271 distribution function. ω_c is the critical threshold of volumetric soil water content w
272 above which root water uptake is reduced in water limited layers of the root zone, but
273 the plant compensates by uptaking more water from other layers that have sufficient
274 available water. Fgc is daily potential dry matter production accounting for the light
275 interception, radiation use efficiency, and the CO_2 effects ($\text{kg hm}^{-2} \text{d}^{-1}$). $AMAX$ is the
276 maximum assimilation rate accounting for temperature effect ($\text{kg hm}^{-2} \text{h}^{-1}$). DL , K_e ,
277 and CC indicate day length (h d^{-1}), extinction coefficient (-) and actual radiation use
278 ($\text{kg hm}^{-2} \text{h}^{-1}$). $Fgass$ is daily actual dry matter production ($\text{kg hm}^{-2} \text{d}^{-1}$) accounting
279 for water ($cf(w)$) and nitrogen stress ($cf(N)$). GAA indicates produced biomass
280 allocated to organs (leaf or grains) ($\text{kg hm}^{-2} \text{d}^{-1}$) with the fraction of $fr(org)$.

281

282 To modify the WHCNS, NCF effects on leaf expansion, photosynthesis rate, and
283 assimilate partition were quantified based on experimental observations and
284 incorporated into WHCNS (Fig. S1). To do so, mean values of observed effects were
285 first calculated by experimental gradient of soil water potential (SWP, negative values)
286 and growth stages (RDS, 0-1) (Table S1-S3). RDS corresponds to planting, tillering,
287 booting, heading, filling, and maturity stages was quantified as 0, 0.20, 0.40, 0.55, 0.75,
288 and 1. Effects at other levels of SWP and RDS were then estimated by bilinear
289 interpolation (i.e., $F^{LAI}(SWP, RDS)$, $F^{Pn}(SWP, RDS)$, $F^{HI}(SWP)$). Three functions were
290 thus developed involving three new genetic parameters to account for differences in
291 cultivar sensitivities (P^{LAI} , P^{Pn} , P^{HI} , Equations 7-9). The three functions were added to
292 the origin crop growth module to modify simulations of leaf area index, net
293 photosynthesis rate and biomass allocated into grains (Equation 10-12, Fig. 2a).

294



$$R^{LAI}(SWP, RDS) = 1 + \left[\left(F^{LAI}(SWP, RDS) \right) - 1 \right] \times P^{LAI} \quad (7)$$

$$R^{Pn}(SWP, RDS) = 1 + \left[\left(F^{Pn}(SWP, RDS) \right) - 1 \right] \times P^{Pn} \quad (8)$$

$$R^{HI}(SWP) = 1 + \left[\left(F^{HI}(SWP) \right) - 1 \right] \times P^{HI} \quad (9)$$

$$LAI' = GAA(leaf) \times SLA \times R^{LAI} \quad (10)$$

$$AMAX' = AMAX \times R^{Pn} \quad (11)$$

$$GAA(grains)' = Fgass \times fr(grains) \times R^{HI} \quad (12)$$

where R^{LAI} , R^{Pn} , R^{HI} represent NCF effects on leaf area index, net photosynthetic rate and harvest index, respectively. SWP represents soil water potential at 15-20 cm soil depth. RDS represents relative development stages (0-1). P^{LAI} , P^{Pn} , and P^{HI} are genetic parameters indicating cultivar sensitivities to irrigation regulation that were calibrated based on observations (Section 2.4). LAI and SLA are leaf area index ($m^2 m^{-2}$) and specific leaf area ($m^2 kg^{-1}$). LAI' , $AMAX'$ and $GAA(grains)'$ denote simulations of the modified model. It is worth noting that the three functions can be flexibly coupled to the other process-based crop models to modify the simulation of leaf area growth, biomass production, and allocation processes. The genetic parameters are needed to be recalibrated against observed yield responses considering different model structures.

2.3.2 Contribution analysis

Scenario simulations were conducted to isolate contributions of the three physiological effects on yield changes ($\Delta Yield$) (Table S4). Four scenarios were simulated by considering all the three effects (S1) and omitting one of the three effects at a time (S2-S4). For each scenario, the model was run under CF and NCF conditions respectively to calculate $\Delta Yield$. The differences in the simulated $\Delta Yield$ between S1 and S2-S4 represent yield changes induced by changes in leaf expansion, photosynthesis rate and assimilate partition, respectively (i.e., $\Delta Yield^{LAI}$, $\Delta Yield^{Pn}$, $\Delta Yield^{HI}$). Relative contribution of each process was calculated as the ratio of the absolute yield change induced by the process to the sum of absolute yield change induced by the three processes (Equation 13).

$$CON^p = \frac{|\Delta Yield^p|}{\sum_{p=1}^3 |\Delta Yield^p|} \times 100 \quad (13)$$

where p represents the three new physiological processes (i.e., $p = 1, 2, 3$), CON^p indicates relative contribution of the process p to $\Delta Yield$, $\Delta Yield^p$ is yield changes induced by the process p .



331 2.4 Parameters regionalization

332

333 Spatially explicit model parameters are critical for reasonably reproducing spatial
334 variabilities of target variables. In this study, seven key model parameters were selected
335 and mapped at 0.5-degree spatial resolution due to their high influence on target
336 variables, including accumulated temperature for crop maturity (*Cumtemp*), minimum
337 assimilation rates (*AMIN*), the maximum CH₄ production rate per soil weight at 30 °C
338 (*MPmax*), maximum portion of denitrification to N₂O production (*f_{N2O_d}*) and the three
339 new genetic parameters (*P^{LAI}*, *P^{Pn}*, *P^{HI}*). These parameters were first finely calibrated at
340 site-scales (Section 2.4.1) and then upscaled to regional scales (Section 2.4.2). To
341 capture spatial variabilities of NCF effects, different parameters were used under CF
342 and NCF conditions, except for genetic parameters. This was consistent with a previous
343 modelling study, aiming to indicate different potentials of methane production and
344 denitrification under different water management regimes (Song et al., 2023).

345

346 2.4.1 Calibration of site-scale parameters

347

348 Under CF conditions, the parameter *Cumtemp* was first determined by cultivar as the
349 minimum cumulative daily temperature higher than 10°C (base temperature for rice
350 growth) across all experiments using the cultivar. Then *AMIN*, *MPmax* and *f_{N2O_d}* were
351 calibrated to achieve the best fit of predicted target variables with observations under
352 continuous flooding conditions (i.e., experimental control). Under NCF conditions,
353 *Cumtemp* and *AMIN* were the same with that calibrated from CF conditions. The other
354 parameters (*MPmax*, *f_{N2O_d}*, *P^{LAI}*, *P^{Pn}* and *P^{HI}*) were then calibrated by minimizing the
355 sum of simulated squared residuals under non-continuous flooding conditions (Table
356 S5). To obtain more accurate parameter estimates, the advanced parameter estimation
357 algorithm (PEST) was used (Doherty, 2010). As a result, 51 groups of genetic
358 parameters (*Cumtemp*, *AMIN*, *P^{LAI}*, *P^{Pn}* and *P^{HI}*), 56 parameter values of *MPmax* (19
359 for control and 37 for treatment) and 24 parameter values of *f_{N2O_d}* (10 for control and
360 14 for treatment) were calibrated.

361

362 2.4.2 Parameters upscaling

363

364 To upscale genetic parameters (*AMIN*, *Cumtemp*, *P^{LAI}*, *P^{Pn}*, *P^{HI}*) calibrated at site
365 scales to regional scales, the rice cultivar for each grid was first determined. Then, the
366 calibrated genetic parameters of the cultivar were used to create the grid. Since the
367 spatial distribution of rice cultivar is unknown, cultivar of each grid cell was
368 determined as follows. First, cultivars with *Cumtemp* lower than the effective
369 accumulative temperature requirement of the grid were identified. This ensures the
370 cultivar could reach maturity under the grid cell's temperature conditions. The grid's
371 temperature requirement was calculated as *Cumtemp* during rice growing periods
372 specified by the crop calendar data of GGCM Phase 3 (Jägermeyr et al., 2021).
373 Subsequently, cultivars with *AMIN* that closely match the baseline *AMIN* of the grid
374 cell were selected. The baseline *AMIN* was estimated using PEST to achieve the best



375 fit of yield simulation with the records in county-scale statistical yearbooks of China
376 (downscaled to 0.5-deg spatial resolution). These procedures were designed to ensure
377 that yield simulations were aligned with cultivar's genetic potential and spatially
378 consistent with observations.

379
380 To upscale parameters MP_{max} and f_{N_2O-d} , two parameter transfer functions (PTFs)
381 were developed. Dependent variables were the ratio of site-calibrated parameters
382 under treatment to that under control (i.e., $R^{MP_{max}}$ and $R^{f_{N_2O-d}}$) (Equation 16-17).
383 Independent variables were determined as field water capacity (FWC) for $R^{MP_{max}}$ and
384 bulk density (BD) for $R^{f_{N_2O-d}}$, due to their higher correlations with dependent
385 variables. The function forms were determined as the form with the highest R^2 . As a
386 result, the relationship between field water capacity and $R^{MP_{max}}$ was best fitted by an
387 exponential function ($R^2 = 0.62$, $p < 0.001$), and the relationship between bulk density
388 and $R^{f_{N_2O-d}}$ was best fitted by a quadratic function ($R^2 = 0.91$, $p < 0.001$) (Fig. S4).
389 The importance of soil properties in regulating spatial heterogeneity of denitrification
390 potentials aligns with previous studies (Tang et al., 2024). Parameters of the PTFs
391 were calibrated using the least square method (Equation 16-17). With the calibrated
392 PTFs, the ratio of parameters under NCF relative to CF ($R^{MP_{max}}$ and $R^{f_{N_2O-d}}$) for each
393 grid could be predicted by combining spatial dataset of FWC and BD . Then gridded
394 MP_{max} and f_{N_2O-d} for CF conditions (MP_{max}^{CF} and $f_{N_2O-d}^{CF}$) were estimated using PEST
395 targeting CH_4 from the EDYGA v8.0 dataset (Crippa et al., 2024) and N_2O emissions
396 estimated by Cui et al. (2024) (Fig. S3). These parameters were estimated for 2013
397 and 2015 and subsequently validated for 2014 and 2016 to assess their ability to
398 reproduce the spatial variability of target variables (Fig. S2). Finally, MP_{max} and f_{N_2O-d}
399 for NCF conditions were calculated by multiplying MP_{max}^{CF} and $f_{N_2O-d}^{CF}$ with the
400 predicted ratio ($R^{MP_{max}}$ and $R^{f_{N_2O-d}}$).

401
402

$$403 \quad R^{MP_{max}} = MP_{max}^{NCF} / MP_{max}^{CF} = 986 \times e^{-26 \times FWC} \quad (16)$$

$$404 \quad R^{f_{N_2O-d}} = f_{N_2O-d}^{NCF} / f_{N_2O-d}^{CF} = 268 \times BD^2 + 789 \times BD + 581 \quad (17)$$

405

406 Where $R^{MP_{max}}$ and $R^{f_{N_2O-d}}$ represent the ratio of parameter MP_{max} and f_{N_2O-d}
407 calibrated under non-continuous flooding (treatment) to that under continuous
408 flooding (control). FWC and BD represent field water capacity ($cm^3 cm^{-3}$) and soil
409 bulk density ($g cm^{-3}$) obtained from SoilGrids (10 km) (Han et al., 2015).

410

411 To prove the efficacy of the PTFs, two other parameter upscaling approaches were also
412 used for comparison, including the mean parameters approach and the spatial proximity
413 approach. These approaches were widely used in previous modelling studies to derive
414 regional parameters and conduct regional simulations (Zhang et al., 2024). To adopt the
415 mean parameter approach, mean value of the site-calibrated MP_{max} and f_{N_2O-d} (Section
416 2.4.1) were calculated respectively for CF and NCF conditions, and then the two



417 constant mean parameters was used in regional simulations. To adopt the spatial
418 proximity approach, the nearest site of a site was first identified according to
419 geographical coordinates. Then both MP_{max} and $f_{N_2O,d}$ calibrated from the nearest site
420 were used for simulation of this site. The three approaches were compared in their
421 performance to reproduce the observed variations in ΔCH_4 and ΔN_2O (Fig. 3).

422

423 2.5 Regional scenario simulations

424

425 Scenario simulations were conducted to test whether the proposed framework could
426 reasonably predict the response sensitivity of target variables and their relations under
427 different irrigation schemes. To do so, the well-calibrated WHCNS model was run
428 under baseline and a series of non-continuous irrigation scenarios using the parallel
429 computing framework (Liang et al., 2023). For baseline condition, irrigation thresholds
430 were set according to Chen et al. (2022). For non-continuous flooding irrigation
431 scenarios, a range of the lowest irrigation threshold levels were set based on
432 observations (-5, -10, -15, -20, -30, -40 and -50 kpa). The upper irrigation thresholds
433 were kept the same with baseline for consistency with experiments. NCF effects were
434 then calculated from model simulations and compared with observed effects. Observed
435 effects were obtained from two datasets. The first is the one compiled for this study
436 (Section 2.2) using soil water potential to distinguish irrigation schemes. The second
437 was obtained from Bo et al. (2022), who used the ratio of days with no surface water to
438 total growing days (UFR) to differentiate irrigation schemes. To facilitate comparison,
439 the UFR of each irrigation scenarios was also calculated and output by WHCNS (Fig.
440 S8).

441

442 2.6 Single-objective and multi-objective optimizations

443

444 Based on scenario simulations, four single-objectives and a multiple-objective were
445 designed to identify optimal irrigation schemes. The four single-objective targets are (1)
446 $maxYield$: maximizing rice yield, (2) $minIRR$: minimizing irrigation water use, (3)
447 $minCH_4$: minimizing CH_4 emission, and (4) $minN_2O$: minimizing N_2O emissions.
448 Under all targets, yield reduction compared to CF conditions was avoided. With optimal
449 solution under the four single-objective scenarios, the largest regulation potentials to
450 increase yield and reduce IRR, CH_4 , and N_2O emissions were assessed. For comparison,
451 the scenario simulations and optimization were also conducted using the origin
452 WHCNS model (Fig. 5).

453

454 The multi-objective optimization was conducted by combining the improved WHCNS
455 model and the NSGA-II algorithm. First, a set of 100 parental populations was
456 initialized with random solutions. Each population includes 1993 individuals,
457 corresponding to 1993 grid cells of irrigated rice areas. Second, the objective functions
458 were computed with each solution by executing the WHCNS model (Equation 18).
459 Third, the performance of each population was evaluated by ranking the fitness of its
460 objective functions. Fitness is a measure of how well a solution performs and is



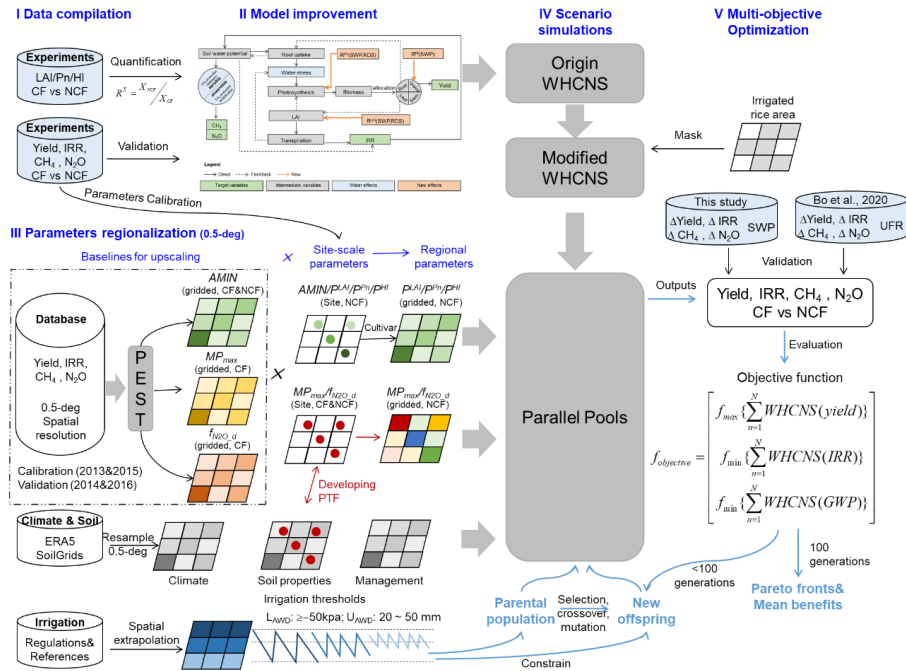
461 calculated based on the non-dominated sorting rank. Then, a new generation was
462 generated through selection, crossover, and mutation based on fitness. Finally, Pareto
463 fronts were generated after 100 generations had been evaluated (that is 10000
464 populations).

465

$$f_{objective} = \begin{bmatrix} f_{max} \left\{ \sum_{n=1}^N WHCNS(yield) \right\} \\ f_{min} \left\{ \sum_{n=1}^N WHCNS(IRR) \right\} \\ f_{min} \left\{ \sum_{n=1}^N WHCNS(GWP) \right\} \end{bmatrix} \quad (18)$$

$$WHCNS(GWP) = 27.2 \times WHCNS(CH_4) + 273 \times WHCNS(N_2O) \quad (19)$$

468 where $f_{objective}(yield, IRR, GWP)$ denotes the collection of objective functions, f_{max}
469 denotes the objective that needs to be maximized (e.g., rice yield), and f_{min} denotes the
470 objective that needs to be minimized (e.g., IRR, GWP). GWP is the integrated global
471 warming potential of combined emissions of CH_4 and N_2O emissions and is
472 calculated based on WHCNS simulations (Equation 19) (Forster et al., 2021). It
473 should be noted that this study set equal weight for each target variable to evaluate the
474 fitness of each solution. Decision-makers can simply set the weight values of different
475 objectives according to their preferences, or adopt advanced multi-objective criteria
476 decision-making methods such as the efficiency coefficient method (Guo et al., 2021).
477 The regulation potentials of multiple-objective optimization were calculated as the
478 averaged NCF effects ($\Delta Yield$, ΔIRR , ΔCH_4 , ΔN_2O , ΔGWP) of all non-dominated
479 solutions. The potentials were further compared with that from single-objective
480 optimizations to investigate tradeoffs between target variables (Fig. 6).
481



482

483 **Figure 1 Research framework of this study.** The framework mainly combines *data*
 484 *compilation, model improvement, parameter regionalization, scenario simulations, and*
 485 *multi-objective optimization.* The framework can be flexibly adapted with alternative
 486 irrigation scenarios, optimization objectives, and optimization algorithms in other
 487 modelling studies. *LAI, Pn,* and *HI* represent leaf area index, net photosynthetic rate,
 488 and harvest index. *AMIN, MPmax, f_{N2O,d}, P^{LAI}, P^{Pn}, and P^{HI}* are model parameters
 489 calibrated and mapped in this study (Section 2.4). *CF* and *NCF* represent continuous
 490 flooding and non-continuous flooding irrigation. *SWP* and *UFR* represent soil water
 491 potential and the ratio of unflooded days to total rice growing days, indicating different
 492 irrigation schemes. See the *Appendix* for detailed descriptions of parameters and
 493 variables.

494

495 3 Results and discussion

496 3.1 Performance of model improvement

497

498 The origin WHCNS model was first evaluated in reproducing variabilities of rice yield
 499 and irrigation water use under various irrigation schemes. For rice yield, model
 500 performance is satisfying when mixing observations under continuous flooding (CF,
 501 experimental control) and non-continuous flooding (NCF, experimental treatments)
 502 irrigation schemes together ($R^2 = 0.41$, normalized root mean square error $nRMSE =$
 503 11%) (Fig. S5). In particular, with fine-tuned crop genetic parameters (i.e., *Cumtemp*
 504 and *AMIN*), the origin model performed well under CF condition ($R^2 = 0.74$, $nRMSE =$
 505 1%), while had worse performance under NCF condition ($R^2 = 0.22$, $nRMSE = 13\%$)

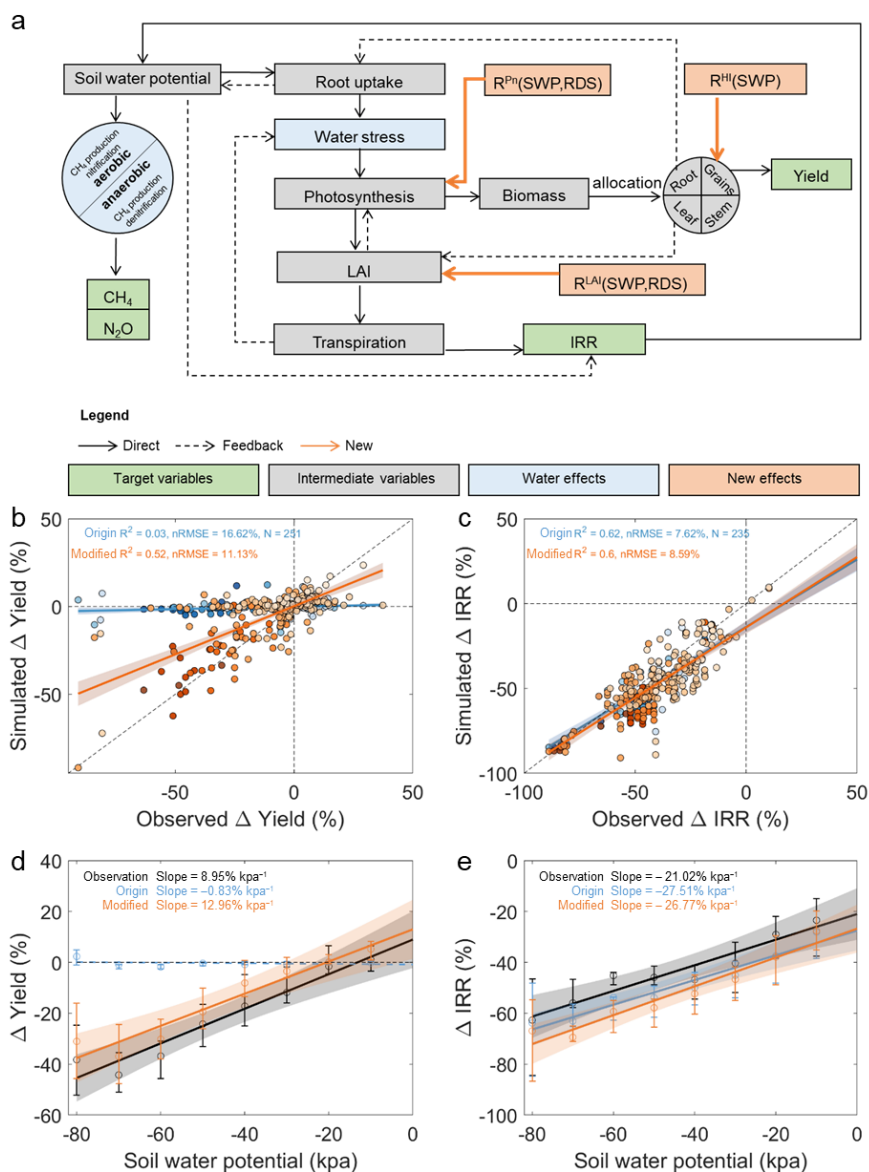


506 (Fig. S5). As a consequence, the origin model failed to reproduce variations in observed
507 yield changes (ΔYield) ($R^2 = 0.03$, $nRMSE = 17\%$) (Fig. 2b). More importantly, the
508 simulations could not reproduce ΔYield sensitivities to soil water potentials presented
509 in field experiments (Fig. 2d). In contrast to yield, model performance in simulating
510 irrigation water use responses (ΔIRR) variabilities and its sensitivities to soil water
511 potentials was acceptable (Fig. 2c and 2e). These results highlight the primary
512 modelling deficiency in simulating ΔYield . Given the satisfying model performance in
513 simulating yield under CF and ΔIRR , the underperformance is likely due to lacking
514 critical physiological processes responsible for yield responses to NCF rather than
515 uncertainties of crop parameters.

516
517 After incorporating the three functions of NCF effects and fine calibration of genetic
518 parameters (Section 2.3, Fig. 2a), the model performance was substantially improved.
519 The explained variabilities of ΔYield increased from 3% to 52% and $nRMSE$ decreased
520 from 17 % to 11% (Fig. 2b). The observed ΔYield sensitivities to soil water potential
521 ($9\% \text{ kpa}^{-1}$, $P < 0.001$) could be reasonably reproduced by the modified model (13%
522 kpa^{-1} , $P < 0.001$) rather than the origin model ($P > 0.05$) (Fig. 2d). The cultivar
523 differences of yield responses could also be simulated ($R = 0.67$) (Fig. S6). Across the
524 three processes, leaf area growth (ΔYield^{LA}) was primarily responsible for yield losses,
525 while net photosynthetic rate (ΔYield^{Pn}) and biomass translocation (ΔYield^{HI})
526 contributed to yield increases (Section 2.3.2, Fig. S7). The positive contributions are
527 larger in warmer and more humid areas, and in acidic soils with larger field water
528 holding capacity and higher SOC. These findings conform with empirical relationships
529 between ΔYield and environmental factors reported by previous meta-analysis (Carrizo
530 et al., 2017). These results prove efficacy of the modified model to predict and regulate
531 ΔYield under diverse irrigation schemes and environmental conditions.

532
533 Besides being coupled to WHCNS as an integrated system, the new functions also
534 contribute to advancing related modelling studies by directly involving positive
535 physiological effects and considering stage-dependent response sensitivities (Li et al.,
536 2017). By contrast, most prevailing crop models only account for negative effects of
537 soil drying and reduced transpiration, while does not incorporating direct compensation
538 effects (such as increased photosynthesis rate upon rewatering). Moreover, constant
539 stress sensitivity parameters were generally used for all growth stages (such as ORYZA
540 and DSSAT) (Bouman et al., 2001; Tsuji et al., 1998). These models could flexibly
541 incorporate the three new functions and recalibrate the genetic parameters (i.e., P^{LA} ,
542 P^{Pn} , and P^{HI}) following the procedures of this study to improve their performance in
543 predicting yield responses.

544



545

546 **Figure 2 Model improvements by incorporating water effects on physiological**
 547 **processes. (a)** Schematic of critical physiological effects in response to different
 548 irrigation schemes and their representation in the WHCNS model. **(b-c)** Model
 549 performance for simulating Δ Yield **(b)** and Δ IRR **(c)** based on the origin (blue) and
 550 modified (orange) WHCNS model. Darker colored dots indicate lower soil water
 551 potential (unit: kpa). **(d-e)** Sensitivity of Δ Yield and Δ IRR to lower irrigation threshold
 552 of soil water potential. Black, blue, and orange colors show the results of observations
 553 and simulations based on the origin and modified WHCNS model, respectively. Circles



554 are mean values; error bars show the 25–75% interquartile range. The lines are the
555 linear regression lines with dashed lines indicating non-significant relationships based
556 on two-sided t-test ($P > 0.05$). The shaded areas around each line represent the 95%
557 confidence interval.

558

559 **3.2 Performance of regionalized parameters**

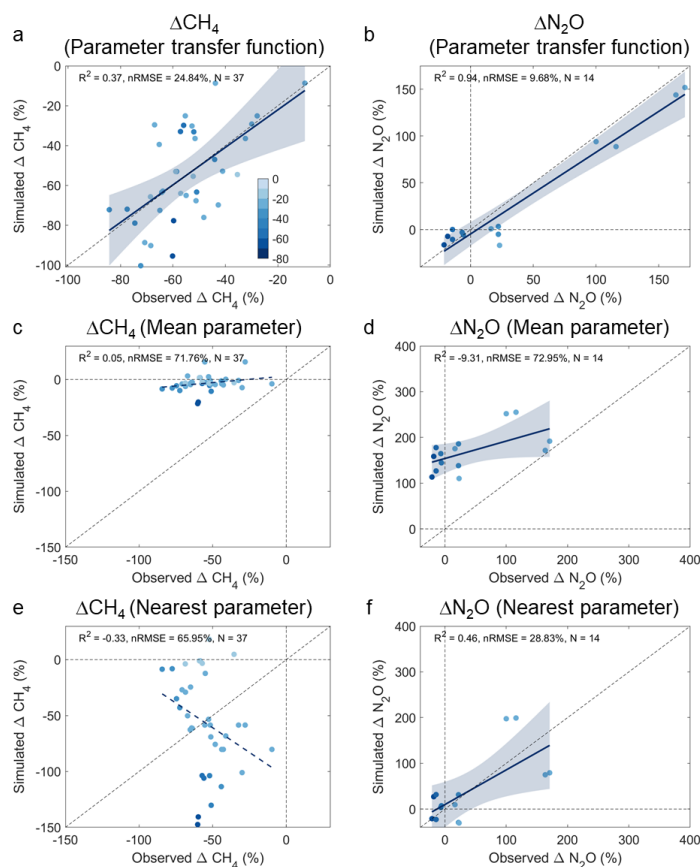
560

561 To simulate regional NCF effects, the model was first run respectively for CF (baseline)
562 and NCF conditions using the parallel computing framework at a spatial resolution of
563 0.5-deg. NCF effects were then calculated using model simulations following Equation
564 1 (Fig.1 and Section 2.4). Using the PEST-calibrated gridded model parameters for CF
565 (Section 2.4.1), the *nRMSE* between model simulations and their spatial datasets were
566 20% to 29% for yield, ~7% for IRR, ~4% for CH₄, and 4% to 6% for N₂O during the
567 validation period (year 2014 and 2016) (Fig.S2). It was noted that the *nRMSE* of rice
568 yield was relatively larger than that of other target variables, despite being within an
569 acceptable range (<30% for the validation periods). This could be caused by interannual
570 cultivar changes, which was difficult to consider in large-scale simulations due to the
571 lack of spatial distribution of rice cultivars. Overall, these results reveal a satisfying
572 model calibration to simulate baseline values and spatial variabilities of target variables.

573

574 To reproduce observed variabilities of NCF effects on target variables, NCF effects on
575 key model parameters (MP_{max} and $f_{N_2O,d}$) were incorporated for constraining model
576 simulations. To do so, NCF effects on model parameters were first quantified from site-
577 scale calibrations and extrapolated to regional scale (Section 2.4). Three approaches of
578 parameter extrapolation were tested and compared, including developing parameter
579 transfer functions (PTFs), using mean site-calibrated parameters (mean), and using
580 spatially nearest calibrated parameters (spatial) (Section 2.4.3). Results showed that
581 developing PTFs performed the best to reproduce observed variabilities of ΔCH_4 and
582 ΔN_2O (Fig. 3). Model simulations using parameters estimated by PTFs explained 37%
583 and 94% of variations in ΔCH_4 and ΔN_2O , with *nRMSE* being 25% for ΔCH_4 and 10%
584 for ΔN_2O (Fig. 3a-b). By contrast, simulations based on the other two approaches could
585 hardly reproduce observed variabilities of ΔCH_4 and ΔN_2O , with *nRMSE* achieving 66%
586 to 72% for ΔCH_4 and 29% to 73% for ΔN_2O (Fig. 3c-f). These results prove the efficacy
587 of the developed PTFs and suggest soil variables as good predictors for spatial
588 extrapolation of site-calibrated parameters to simulate CH₄ and N₂O. The PTFs could
589 also be referred by other biogeochemical models for regional simulations of CH₄ and
590 N₂O (such as DNDC and DLEM) (Zhang et al., 2016).

591



592
 593 **Figure 3 Comparison of model parameter upscaling approaches.** Model
 594 performance in simulating methane and nitrous oxide emissions changes based on
 595 parameters derived from **(a-b)** parameter transfer functions (PTFs), **(c-d)** mean site-
 596 calibrated parameters, and **(e-f)** spatially nearest parameters. The color of the dots
 597 indicates lower irrigation thresholds of soil water potential under non-continuous
 598 flooding irrigation (unit: kpa). The solid lines are regression lines with dashed lines
 599 indicating non-significant relationships ($P > 0.05$). Blue shading around each line
 600 represents the 95% confidence interval.

601
 602 Considering scarce observations of NCF effects across space, it was impractical to
 603 directly evaluate the regionalized parameters in reproducing spatial variability of
 604 NCF effects. Therefore, the proposed framework was evaluated in terms of the response
 605 sensitivity of target variables and their relationships under different irrigation schemes
 606 (Section 2.5). Scenario simulations broadly conformed with observations regarding the
 607 magnitude of NCF effects and response sensitivity across soil water potential gradients
 608 (Fig. S8). With decreased soil water potential threshold, ΔYield decreased quasi-linearly,
 609 ΔCH_4 and ΔIRR decreased at a decelerating rate, while $\Delta\text{N}_2\text{O}$ showed slight variabilities
 610 (Fig. S8a). The decelerating decrease in ΔCH_4 was also observed in experiments,



611 suggesting the model ability to simulate maximum potentials of CH₄ mitigation
612 (Balaine et al., 2019). The response sensitivity was further validated using an alternative
613 observation dataset (Fig. S8b). Besides, the observed synergy or tradeoffs of the yield-
614 IRR-GHG nexus were broadly covered by scenario simulations using the modified
615 model rather than using the origin model (Fig. S8c). Such bias could further impact
616 assessment of regulation potentials of the food-water-climate nexus.

617

618 3.3 Assessment of regional regulation potentials

619

620 Scenario simulations revealed large spatial variabilities of NCF effects on all target
621 variables (Fig. 4). Applying the the same irrigation scheme (e.g., lower irrigation
622 threshold of -15 or -30 kpa) could induce larger yield increase in southwest single-
623 rice regions (XNS: 2.4% to 3.4%), while larger yield losses in northern regions
624 (HHH: -3.2%) (Fig. 4a and b). The HHH region also showed larger yield sensitivity
625 with decreased lower irrigation threshold (-0.24% kpa⁻¹) (Fig. 4c). For IRR,
626 relatively larger water saving benefits occurred in south regions, whereas response
627 sensitivity was larger in northeast regions (-1.7% kpa⁻¹). For CH₄, north rice growing
628 regions showed relatively higher reductions (NES: 64% to 82%, HHH: 77% to 88%)
629 and higher response sensitivity to decreased soil water potential threshold. The
630 findings about larger water saving benefits in south China and larger CH₄ mitigation
631 in north China were consistent with previous assessments (Tian et al., 2021).
632 However, N₂O emissions showed widespread increase regardless of lower irrigation
633 threshold, except for northeast regions, indicating low opportunities to reduce N₂O by
634 only optimizing water management.

635

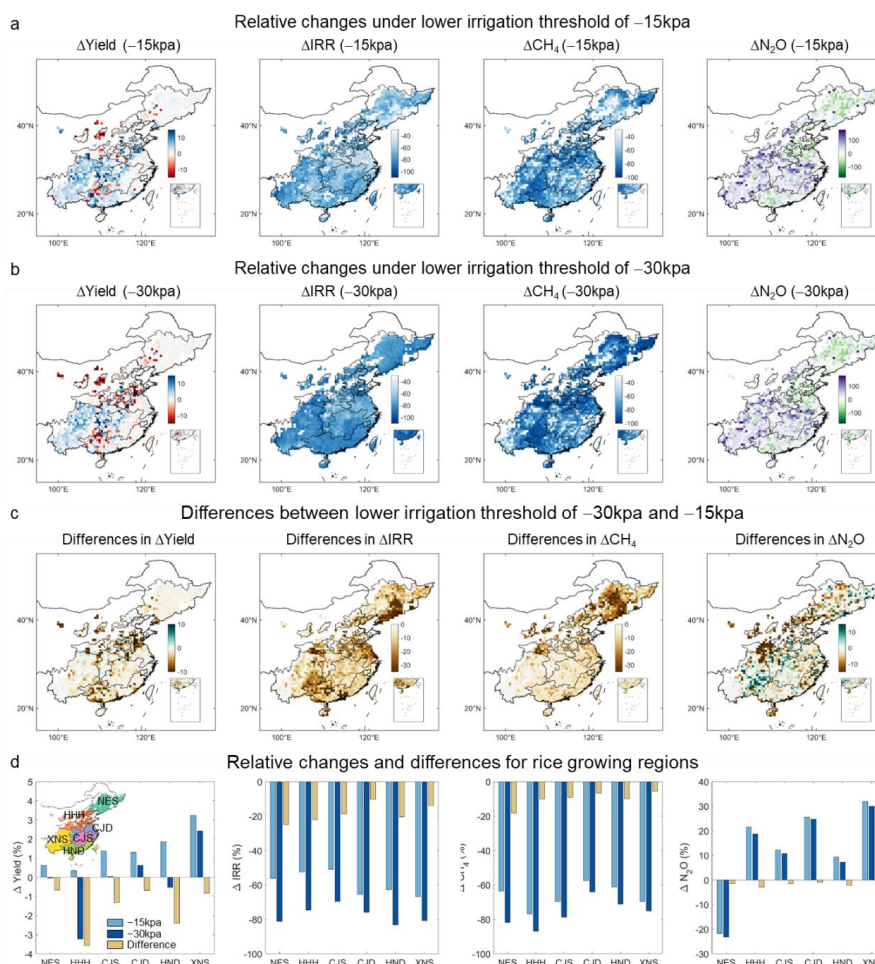
636 Four single objective targets were designed to identify the largest regulation potentials
637 from NCF adoption, including maximizing rice yield, minimizing IRR, CH₄
638 emissions, or N₂O emissions (denoted as *maxYield*, *minIRR*, *minCH₄*, *min N₂O*,
639 Section 2.6). Results indicated that the largest regulation potentials of Δ Yield, Δ IRR,
640 Δ CH₄ and Δ N₂O were 4.6%, -61.0%, -64.2% and -10.9%, respectively (Fig. 5a).
641 These potentials could be achieved respectively over 91%, 91%, 88% and 26% of
642 national rice areas (Fig. 5b). Spatially, larger yield increase potential occurred in south
643 (HND: 7.7%) and southwest regions (XNS: 6.8%) (Fig. S9A). The reduction potential
644 of IRR and CH₄ showed relatively slight spatial variabilities. In contrast, reduction
645 potential of N₂O primarily concentrated in northern regions (NES: -30%) due to
646 increased N₂O in southern regions (Fig. 5a and S9A). N₂O increase in southern
647 regions is associated with higher nitrogen application rates, providing substrate for
648 nitrification and denitrification processes to facilitate N₂O emissions (Jiang et al.,
649 2019). The results conform to previous studies in that irrigation and nitrogen should
650 be co-regulated for these areas to avoid unintended N₂O emissions from water
651 management (Jiang et al., 2019; Kritee et al., 2018).

652

653 The largest regulation potentials of Δ Yield, Δ IRR, Δ CH₄, and Δ N₂O are not likely to
654 be achieved at the same time, as evidenced by different optimized irrigation strategies



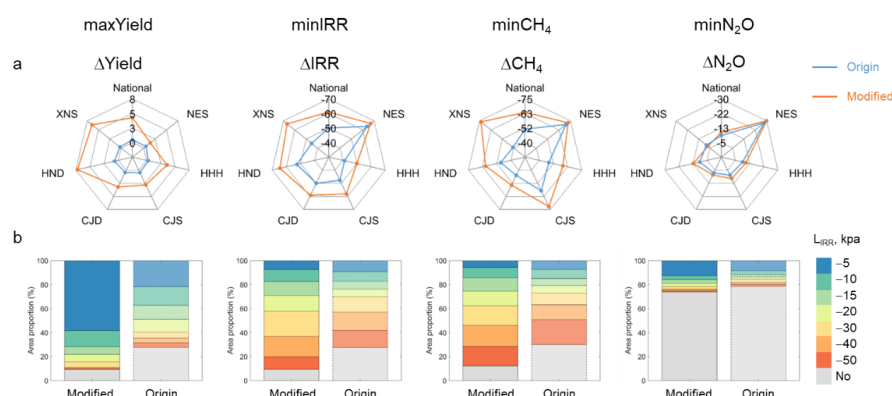
655 between single-objective targets (Fig. 5 and S10). For example, the lower irrigation
 656 threshold should be higher than -20kpa for most areas (84%) under *maxYield*, while
 657 lower than -20kpa over half areas under *minIRR* and *minCH₄*. This suggests tradeoffs
 658 between yield increase and IRR/*CH₄* mitigation (Bo et al., 2021). To compare, using
 659 the origin model could overlook nearly 20% feasible areas for applying optimized
 660 irrigation schemes (Fig. 5). As a consequence, regulation potentials of ΔYield , ΔIRR ,
 661 ΔCH_4 and $\Delta\text{N}_2\text{O}$ could be underestimated by 4%, 11%, 14%, and 2%, especially for
 662 the southwest regions (XNS) (Fig. 5a). Moreover, optimal NCF strategies also
 663 differed from that identified by the improved model, particular under *maxYield* targets
 664 (Fig. 5b). These results showed important implications of the improved framework for
 665 prompting sustainable water management.
 666



667
 668 **Figure 4 Spatial pattern of relative changes in target variables under different**
 669 **irrigation schemes and differences.** The four columns correspond to the four target
 670 variables ΔYield , ΔIRR , ΔCH_4 , and $\Delta\text{N}_2\text{O}$, respectively. (a) relative changes of target



671 variables under a lower irrigation potential of -15 kpa, **(a)** relative changes of target
 672 variables under a lower irrigation potential of -30 kpa, **(c)** differences between (b) and
 673 (a), **(d)** results for different rice growing regions. NES, HHH, CJS, CJD, HND, and
 674 XNS indicate six rice growing areas of China, namely, Northeast Single rice,
 675 HuangHuaiHai single rice, Yangtze River single rice, Yangtze River double Rice, South
 676 China Double rice, and Southwest China Single rice, respectively.
 677



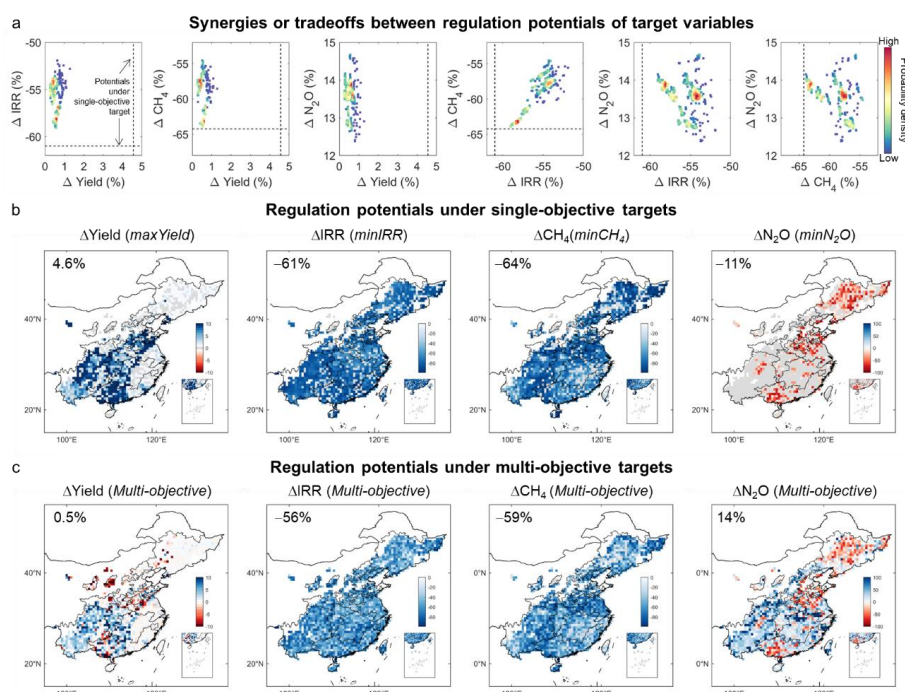
678
 679 **Figure 5 Comparison of the origin and modified model from (a) regulation**
 680 **potentials and (b) optimized irrigation schemes under single-objective targets.**
 681 The four columns show results under four single objective targets: maximizing rice
 682 yield (*maxYield*), minimizing irrigation water use (*minIRR*), minimizing CH₄
 683 emissions (*minCH₄*), and minimizing N₂O emissions (*maxN₂O*). **(a)** Area-weighted
 684 Δ Yield, Δ IRR, Δ CH₄, and Δ N₂O for China and six rice growing regions. Blue and
 685 orange indicate results from the origin and modified model, respectively. **(b)**
 686 Proportions of rice areas with corresponding optimized lower irrigation thresholds
 687 (L_{IRR}) to total irrigated rice areas under the four single objective targets. NES, HHH,
 688 CJS, CJD, HND, and XNS indicate six rice growing areas of China, namely,
 689 Northeast Single rice, HuangHuaiHai single rice, Yangtze River single rice, Yangtze
 690 River double Rice, South China Double rice, and Southwest China Single rice,
 691 respectively.

692 3.4 Tradeoffs between food, water, and greenhouse gas emissions

695 The NSGA-II algorithm was conducted to investigate synergies or tradeoffs of the food-
 696 water-climate nexus (Fig. 6 and Section 2.6). There were evident tradeoffs between
 697 reducing CH₄ (or IRR) and N₂O (Fig. 6a). In contrast, synergies were noted between
 698 reducing IRR and CH₄, as well as between inhibiting N₂O emissions and increasing rice
 699 yield. The relationships between yield increase and CH₄ (or IRR) reductions were more
 700 complicated due to the impacts of varying irrigation timing and no-flooded days (Yan
 701 et al., 2024). Adopting non-dominated solutions from multi-objective optimization
 702 could realize over 90% of the largest reduction potentials of IRR and CH₄, while at the
 703 cost of 4% less yield increase (4.6% versus 0.5%) and 25% higher nitrous dioxide



704 emissions (−11% versus 14%). The N₂O increase is because this study used integrated
 705 warming potentials of CH₄ and N₂O emissions (GWP) to indicate greenhouse gas
 706 emissions so that CH₄ outweighed N₂O due to large emission quantities (Section 2.6).
 707 Since the multi-objective optimization was conducted targeting national optimum of
 708 food-water-GHGs, NCF practices were adopted in the south regions to realize more
 709 considerable IRR and CH₄ reductions contributing to larger national co-benefits. Noted
 710 that other objective functions could also be designed for multi-objective optimization,
 711 such as applying other indicators (e.g., water productivity, yield-scaled GWP), setting
 712 distinguished weights for each indicator or grid cell.
 713



714
 715 **Figure 6 Regulation potentials of Δ Yield, Δ IRR, Δ CH₄, and Δ N₂O under single-**
 716 **objective and multi-objective targets. (a)** Synergies or tradeoffs between target
 717 variables with different solutions of multi-objective optimization. Dots color indicates
 718 probability density distributions of variable changes from all non-dominated solutions
 719 (N = 10000) of the NSGA II optimization. The vertical and horizontal dashed lines
 720 show national regulation potentials of the target variable under single-objective
 721 targets, with corresponding spatial distributions presented in panel (b). Note that the
 722 results of Δ N₂O potentials (−11%) were not shown in the third, fifth, and sixth
 723 subplots for a clearer view. **(b)** Δ Yield, Δ IRR, Δ CH₄, and Δ N₂O under single-objective
 724 targets of maximizing rice yield (*maxYield*), minimizing irrigation water use
 725 (*minIRR*), minimizing CH₄ emissions (*minCH₄*), and minimizing N₂O emissions
 726 (*maxN₂O*). These results indicate the maximum benefits of each target variable from
 727 adopting non-continuous irrigation, which could not be necessarily realized



728 simultaneously. (c) Δ Yield, Δ IRR, Δ CH₄, and Δ N₂O under multi-objective
729 optimization. These figures show mean benefits from all non-dominated solutions of
730 the NSGA II optimization (N = 10000).

731

732 **3.5 Uncertainties and future direction**

733

734 This framework is subject to several uncertainties, mainly sourced from observational
735 gaps and management-related input data. First, the absence of field observations for
736 baseline CH₄ and N₂O emissions across regional scales forced us to use estimates from
737 inventory or data-driven approaches as a proxy for deriving gridded model parameters
738 of this study (Cui et al., 2021; Crippa et al., 2024). Despite uncertainties in predicting
739 absolute values, these parameters could reasonably reproduce the spatial patterns and
740 could be further refined given increased field observations. Second, the limited
741 experimental observations of CH₄ ($n = 37$) and N₂O ($n = 14$) under various irrigation
742 schemes have contributed to uncertainties in developing and applying parameter
743 transfer functions (PTFs). The values of PTFs predictors (bulk density and field water
744 capacity) in the observation dataset (1.34~1.48 g cm⁻³ and 0.25~0.30 cm³ cm⁻³) did not
745 encompass the full range across national rice areas (1.24~1.48 g cm⁻³ and 0.22~0.32
746 cm³ cm⁻³), indicating potential extrapolation in parameters regionalization. Despite
747 these uncertainties, the PTFs significantly improved over previous approaches
748 (constant parameters or spatial proximity approach). Lastly, current irrigation practices
749 across large scales remain largely unknown, so that irrigation thresholds were set
750 following previous recommendations. However, actual farmer practices are influenced
751 by various factors and may not align with these recommendations. This discrepancy
752 could lead to an overestimation or underestimation of target variables and further
753 introduce uncertainties to the assessment of regulation potentials.

754

755 These uncertainties provide insights to enlighten future research efforts, including
756 conducting extensive observations and experiments and developing high-resolution
757 input data. On the one hand, intensive GHGs monitoring networks are essential to
758 reduce uncertainties associated with parametrization (Arenas-Calle et al., 2024). To
759 better constrain the PTFs and reduce extrapolation uncertainty, field experiments
760 combined with incubation experiments covering a broad range of soil properties,
761 including bulk density and field water capacity, should be conducted. In addition,
762 extensive field experiments with simultaneous measurements of yield, IRR, CH₄, and
763 N₂O emissions across diverse environments are required to validate the framework
764 further. On the other hand, developing a high-resolution dataset of current irrigation
765 schemes is crucial for more accurate model parameter calibration and realistic
766 assessment of regulation potentials. This could be achieved by integrating remote
767 sensing technologies with extensive field investigations (Novick et al., 2022).

768

769 **4 Conclusion**

770

771 This study introduced an advancing framework for process-based modelling of the



772 complex food-water-climate nexus in rice fields under various water management
 773 schemes. By integrating the Soil Water Heat Carbon Nitrogen Simulator (WHCNS)
 774 with key physiological effects, a novel model upscaling method, and the NSGA-II
 775 multi-objective optimization algorithm at a parallel computing platform, the framework
 776 provides a comprehensive approach to optimize irrigation strategies. Applying this
 777 framework to China's rice cropping system, we assessed the largest regulation
 778 potentials of Δ Yield, Δ IRR, Δ CH₄, and Δ N₂O as 4.6%, -61.0%, -64.2%, and -10.9%
 779 from 91%, 91%, 88%, and 26% of national rice areas. However, these regulation
 780 potentials could not be simultaneously realized due to complicated tradeoffs among
 781 food-water-GHGs. Based on NSGA II multi-objective optimization targeting food-
 782 water-GHGs co-benefits, over 90% of the reduction potentials in water use and methane
 783 emissions could be realized, while at the cost of 4% less yield increase and 25% higher
 784 nitrous dioxide emissions. The proposed framework is a valuable tool for irrigation
 785 optimization in rice cultivation and also offers a transferable paradigm for incorporating
 786 other management effects into process-based models, thus supporting comprehensive
 787 assessments of sustainable management measures.

788
 789
 790

Appendix: abbreviation table

Type	Abbreviation	Description
Target variables	<i>Yield</i>	rice yield (kg ha ⁻¹)
	<i>IRR</i>	irrigation water use (mm)
	<i>CH₄</i>	methane emissions (kg ha ⁻¹)
	<i>N₂O</i>	nitrous oxide emissions (kg ha ⁻¹)
	<i>GWP</i>	integrated global warming potential of CH ₄ and N ₂ O at 100-year scale, calculated as 27.2×CH ₄ +273×N ₂ O (kg ha ⁻¹)
	<i>LAI</i>	leaf area index (m ² m ⁻²)
	<i>Pn</i>	net photosynthetic rate (kg ha ⁻¹)
	<i>HI</i>	harvest index (-)
Effect sizes	$R^{Yield}, R^{IRR}, R^{CH_4}, R^{N_2O}, R^{LAI}, R^{Pn}, R^{HI}$	Effect size of non-continuous flooding irrigation (NCF) on target variables, calculated as the ratio of observations under NCF to that under continuous flooding (CF) (-)
Relative changes	$\Delta Y_{ield}, \Delta IRR, \Delta CH_4, \Delta N_2O$	Relative changes of target variables under NCF compared to CF, calculated as (R-1)×100 (%)
Model parameters	<i>Cumtemp</i>	accumulated temperature for crop maturity (°C)
	<i>AMIN</i>	minimum assimilation rates (kg hm ⁻² h ⁻¹)
	p^{LAI}, p^{Pn}, p^{HI}	genetic parameters accounting for cultivar sensitivities to NCF effects on leaf area index, net photosynthetic rate, and harvest index
	<i>MPmax</i>	maximum CH ₄ production rate per soil weight at 30 °C (g C g ⁻¹ d ⁻¹)
	$f_{N_2O\ d}$	maximum portion of denitrification to N ₂ O



		production (-)
Environmental variables	T	mean daily air temperature during rice growing season ($^{\circ}\text{C}$)
	P	total precipitation during rice growing season (mm)
	$PETc$	total crop evapotranspiration during rice growing season (mm)
	CWA	climatological water availability, calculated as the difference between P and $PETc$ ($P-PETc$, mm)
Soil variables	BD	bulk density (g cm^{-3})
	$Sand$	sand content (%)
	SOC	soil organic carbon (%)
	SAT	saturated water content ($\text{cm}^3 \text{cm}^{-3}$)
	FWC	field water capacity ($\text{cm}^3 \text{cm}^{-3}$)
Management variables	L_{AWD}	lower irrigation threshold, indicated by SWP (kpa)
	U_{AWD}	upper irrigation threshold (cm)
	SWP	soil water potential (kpa)
	UFR	ratio of unflooded days to total growing days (%)
Optimization objectives	$maxYield$	maximizing rice yield
	$minIRR$	minimizing irrigation water use
	$minCH_4$	minimizing CH_4 emission
	$minN_2O$	minimizing N_2O emissions

791

792 **Code and data availability**

793 The executable WHCNS model and required model input files are available at
 794 <https://figshare.com/s/139f3ad8a70faa99724d>. Spatial dataset of harvested area of
 795 irrigated rice is available from <https://doi.org/10.7910/DVN/KAGRFI>. Climate data is
 796 available from <https://cds.climate.copernicuseu/cdsapp#!/search?type=dataset>. Soil
 797 data are available from <http://globalchange.bnu.edu.cn/research/data>. Crop calendar
 798 data are available from <https://zenodo.org/record/5062513>. All other data that support
 799 the findings of this study are available in the main text or the Supplementary
 800 Information.

801

802 **Acknowledgements**

803 This study was supported by the National Natural Science Foundation of China
 804 (42225102, 42361144876, F.Z.).

805

806 **Author contributions**

807 F.Z. designed the study. Y.B. and H.L. performed all computational analyses. Y.B.,
 808 H.L. and F.Z. drafted the paper. Y.B., H.L., T. L. and F.Z. reviewed and commented on
 809 the manuscript.

810



811 **Conflict of interest statement**

812 The authors declare no conflicts of interest.

813

814 **Reference**

- 815 The world bank. Water resources management.
816 (<https://www.worldbank.org/en/topic/waterresourcesmanagement>), 2017.
- 817 Arenas-Calle, L., Sherpa, S., Rossiter, D., Nayak, H., Urfels, A., Kritee, K., Poonia, S.,
818 Singh, D. K., Choudhary, A., Dubey, R., Kumar, V., Nayak, A. K., and
819 McDonald, A.: Hydrologic variability governs GHG emissions in rice-based
820 cropping systems of Eastern India, *Agr Water Manage*, 301, 108931,
821 <https://doi.org/10.1016/j.agwat.2024.108931>, 2024.
- 822 Balaine, N., Carrijo, D. R., Adviento-Borbe, M. A., and Linquist, B.: Greenhouse Gases
823 from Irrigated Rice Systems under Varying Severity of Alternate-Wetting and
824 Drying Irrigation, *Soil Science Society of America Journal*, 83, 1533-1541,
825 <https://doi.org/10.2136/sssaj2019.04.0113>, 2019.
- 826 Bo, Y., Jägermeyr, J., Yin, Z., Jiang, Y., Xu, J., Liang, H., and Zhou, F.: Global benefits
827 of non-continuous flooding to reduce greenhouse gases and irrigation water use
828 without rice yield penalty, *Global Change Biology*, 28, 3636-3650,
829 <https://doi.org/10.1111/gcb.16132>, 2022.
- 830 Bo, Y., Zhou, F., Zhao, J., Liu, J., Liu, J., Ciais, P., Chang, J., and Chen, L.: Additional
831 surface-water deficit to meet global universal water accessibility by 2030, *J*
832 *Clean Prod*, 320, 128829, <https://doi.org/10.1016/j.jclepro.2021.128829>, 2021.
- 833 Bouman, B. A. M., Kropff, M., Tuong, T. P., Wopereis, M. C. S., Berge, H. F. M. t., and
834 Laar, H. H. V.: ORYZA2000 : modeling lowland rice,
- 835 Carlson, K. M., Gerber, J. S., Mueller, N. D., Herrero, M., MacDonald, G. K., Brauman,
836 K. A., Havlik, P., O'Connell, C. S., Johnson, J. A., Saatchi, S., and West, P. C.:
837 Greenhouse gas emissions intensity of global croplands, *Nature Climate*
838 *Change*, 7, 63-68, 10.1038/nclimate3158, 2017.
- 839 Carrijo, D. R., Lundy, M. E., and Linquist, B. A.: Rice yields and water use under
840 alternate wetting and drying irrigation: A meta-analysis, *Field Crop Res*, 203,
841 173-180, 2017.
- 842 Chen, M., Linker, R., Wu, C., Xie, H., Cui, Y., Luo, Y., Lv, X., and Zheng, S.: Multi-
843 objective optimization of rice irrigation modes using ACOP-Rice model and
844 historical meteorological data, *Agr Water Manage*, 272, 107823,
845 <https://doi.org/10.1016/j.agwat.2022.107823>, 2022.
- 846 Crippa, M., Guizzardi, D., Pagani, F., Schiavina, M., Melchiorri, M., Pisoni, E.,
847 Graziosi, F., Muntean, M., Maes, J., Dijkstra, L., Van Damme, M., Clarisse, L.,
848 and Coheur, P.: Insights into the spatial distribution of global, national, and
849 subnational greenhouse gas emissions in the Emissions Database for Global
850 Atmospheric Research (EDGAR v8.0), *Earth Syst. Sci. Data*, 16, 2811-2830,
851 10.5194/essd-16-2811-2024, 2024.
- 852 Cui, X., Zhou, F., Ciais, P., Davidson, E. A., Tubiello, F. N., Niu, X., Ju, X., Canadell,
853 J. G., Bouwman, A. F., Jackson, R. B., Mueller, N. D., Zheng, X., Kanter, D. R.,
854 Tian, H., Adalibieke, W., Bo, Y., Wang, Q., Zhan, X., and Zhu, D.: Global



- 855 mapping of crop-specific emission factors highlights hotspots of nitrous oxide
856 mitigation, *Nature Food*, 2, 886-893, 10.1038/s43016-021-00384-9, 2021.
- 857 Doherty, J.: PEST: Model Independent Parameter Estimation, 2010.
- 858 Feddes, R. A. and Zaradny, H.: Model for simulating soil-water content considering
859 evapotranspiration — Comments, *Journal of Hydrology*, 37, 393-397,
860 [https://doi.org/10.1016/0022-1694\(78\)90030-6](https://doi.org/10.1016/0022-1694(78)90030-6), 1978.
- 861 Flörke, M., Schneider, C., and McDonald, R. I.: Water competition between cities and
862 agriculture driven by climate change and urban growth, *Nature Sustainability*,
863 1, 51-58, 10.1038/s41893-017-0006-8, 2018.
- 864 Forster, P., T. Storelvmo, Armour, K., Collins, W., Dufresne, J. L., Frame, D., Lunt, D.
865 J., Mauritsen, T., Palmer, M. D., Watanabe, M., Wild, M., and Zhang, H.: The
866 Earth's Energy Budget, Climate Feedbacks, and Climate Sensitivity. In: *Climate*
867 *Change 2021: The Physical Science Basis. Contribution of Working Group I to*
868 *the Sixth Assessment Report of the Intergovernmental Panel on Climate Change*
869 [Masson-Delmotte, V., P. Zhai, A. Pirani, S. L. Connors, C. Péan, S. Berger, N.
870 Caud, Y. Chen, L. Goldfarb, M. I. Gomis, M. Huang, K. Leitzell, E. Lonnoy,
871 J.B.R. Matthews, T. K. Maycock, T. Waterfield, O. Yelekçi, R. Yu and B. Zhou
872 (eds.)]. Cambridge University Press. In Press., 2021.
- 873 Guo, D., Olesen, J. E., Manevski, K., and Ma, X.: Optimizing irrigation schedule in a
874 large agricultural region under different hydrologic scenarios, *Agr Water*
875 *Manage*, 245, 106575, <https://doi.org/10.1016/j.agwat.2020.106575>, 2021.
- 876 Han, E. I., Amor; Koo, Jawoo "Global High-Resolution Soil Profile Database for Crop
877 Modeling Applications", <http://dx.doi.org/10.7910/DVN/1PEEY0>, Harvard
878 Dataverse, V1, 2015.
- 879 Hersbach, H., Bell, B., Berrisford, P., Biavati, G., Horányi, A., Muñoz Sabater, J.,
880 Nicolas, J., Peubey, C., Radu, R., Rozum, I., Schepers, D., Simmons, A., Soci,
881 C., Dee, D., Thépaut, J.-N.: ERA5 hourly data on single levels from 1979 to
882 present. Copernicus Climate Change Service (C3S) Climate Data Store (CDS).
883 (Accessed on < 06-10-2021>), 10.24381/cds.adbb2d47, 2018.
- 884 Ishfaq, M., Farooq, M., Zulfiqar, U., Hussain, S., Akbar, N., Nawaz, A., and Anjum, S.
885 A.: Alternate wetting and drying: A water-saving and ecofriendly rice
886 production system, *Agr Water Manage*, 241, 106363,
887 <https://doi.org/10.1016/j.agwat.2020.106363>, 2020.
- 888 Jägermeyr, J., Müller, C., Ruane, A. C., Elliott, J., Balkovic, J., Castillo, O., Faye, B.,
889 Foster, I., Folberth, C., Franke, J. A., Fuchs, K., Guarin, J. R., Heinke, J.,
890 Hoogenboom, G., Iizumi, T., Jain, A. K., Kelly, D., Khabarov, N., Lange, S.,
891 Lin, T.-S., Liu, W., Mialyk, O., Minoli, S., Moyer, E. J., Okada, M., Phillips, M.,
892 Porter, C., Rabin, S. S., Scheer, C., Schneider, J. M., Schyns, J. F., Skalsky, R.,
893 Smerald, A., Stella, T., Stephens, H., Webber, H., Zabel, F., and Rosenzweig, C.:
894 Climate impacts on global agriculture emerge earlier in new generation of
895 climate and crop models, *Nature Food*, 2, 873-885, 10.1038/s43016-021-00400-
896 y, 2021.
- 897 Jiang, W., Huang, W., Liang, H., Wu, Y., Shi, X., Fu, J., Wang, Q., Hu, K., Chen, L.,
898 Liu, H., and Zhou, F.: Is rice field a nitrogen source or sink for the environment?,



- 899 Environmental Pollution, 283, 117122,
900 <https://doi.org/10.1016/j.envpol.2021.117122>, 2021.
- 901 Jiang, Y., Carrijo, D., Huang, S., Chen, J., Balaine, N., Zhang, W. J., van Groenigen, K.
902 J., and Linquist, B.: Water management to mitigate the global warming potential
903 of rice systems: A global meta-analysis, *Field Crop Res*, 234, 47-54, 2019.
- 904 Kritee, K., Nair, D., Zavala-Araiza, D., Proville, J., Rudek, J., Adhya, T. K., Loecke, T.,
905 Esteves, T., Balireddygar, S., Dava, O., Ram, K., S. R., A., Madasamy, M.,
906 Dokka, R. V., Anandaraj, D., Athiyaman, D., Reddy, M., Ahuja, R., and
907 Hamburg, S. P.: High nitrous oxide fluxes from rice indicate the need to manage
908 water for both long- and short-term climate impacts, *Proceedings of the
909 National Academy of Sciences*, 115, 9720-9725, doi:10.1073/pnas.1809276115,
910 2018.
- 911 Lampayan, R. M., Rejesus, R. M., Singleton, G. R., and Bouman, B. A. M.: Adoption
912 and economics of alternate wetting and drying water management for irrigated
913 lowland rice, *Field Crop Res*, 170, 95-108, 2015.
- 914 Li, T., Angeles, O., Marcaida, M., Manalo, E., Manalili, M. P., Radanielson, A., and
915 Mohanty, S.: From ORYZA2000 to ORYZA (v3): An improved simulation
916 model for rice in drought and nitrogen-deficient environments, *Agricultural and
917 Forest Meteorology*, 237-238, 246-256,
918 <https://doi.org/10.1016/j.agrformet.2017.02.025>, 2017.
- 919 Liang, H., Yang, S., Xu, J., and Hu, K.: Modeling water consumption, N fates, and rice
920 yield for water-saving and conventional rice production systems, *Soil and
921 Tillage Research*, 209, 104944, <https://doi.org/10.1016/j.still.2021.104944>,
922 2021.
- 923 Liang, H., Hu, K., Qi, Z., Xu, J., and Batchelor, W. D.: A distributed agroecosystem
924 model (RegWHCNS) for water and N management at the regional scale: A case
925 study in the North China Plain, *Computers and Electronics in Agriculture*, 213,
926 108216, <https://doi.org/10.1016/j.compag.2023.108216>, 2023.
- 927 Liang, H., Xu, J., Hou, H., Qi, Z., Yang, S., Li, Y., and Hu, K.: Modeling CH₄ and N₂O
928 emissions for continuous and noncontinuous flooding rice systems, *Agr Syst*,
929 203, 103528, <https://doi.org/10.1016/j.agsy.2022.103528>, 2022.
- 930 Novick, K. A., Ficklin, D. L., Baldocchi, D., Davis, K. J., Ghezzehei, T. A., Konings,
931 A. G., MacBean, N., Raoult, N., Scott, R. L., Shi, Y. N., Sulman, B. N., and
932 Wood, J. D.: Confronting the water potential information gap, *Nat Geosci*, 15,
933 158-164, 2022.
- 934 Song, H., Zhu, Q. a., Blanchet, J.-P., Chen, Z., Zhang, K., Li, T., Zhou, F., and Peng, C.:
935 Central Role of Nitrogen Fertilizer Relative to Water Management in
936 Determining Direct Nitrous Oxide Emissions From Global Rice-Based
937 Ecosystems, *Global Biogeochemical Cycles*, 37, 2023.
- 938 Tan, J., Zhao, S., Liu, B., Luo, Y., and Cui, Y.: Global sensitivity analysis and
939 uncertainty analysis for drought stress parameters in the ORYZA (v3) model,
940 *Agronomy Journal*, 113, 1407-1419, <https://doi.org/10.1002/agj2.20580>, 2021.
- 941 Tang, Y., Su, X., Wen, T., McBratney, A. B., Zhou, S., Huang, F., and Zhu, Y.-g.: Soil
942 properties shape the heterogeneity of denitrification and NO emissions across



- 943 large-scale flooded paddy soils, *Global Change Biology*, 30, e17176,
944 <https://doi.org/10.1111/gcb.17176>, 2024.
- 945 Tian, Z., Fan, Y. D., Wang, K., Zhong, H. L., Sun, L. X., Fan, D. L., Tubiello, F. N., and
946 Liu, J. G.: Searching for "Win-Win" solutions for food-water-GHG emissions
947 tradeoffs across irrigation regimes of paddy rice in China, *Resour Conserv Recy*,
948 166, 2021.
- 949 Tsuji, G. Y., Hoogenboom, G., and Thornton, P. K.: Understanding Options for
950 Agricultural Production, *Systems Approaches for Sustainable Agricultural*
951 *Development*,
- 952 Xu, J. Z., Liao, Q., Yang, S. H., Lv, Y. P., Wei, Q., Li, Y. W., and Hameed, F.: Variability
953 of Parameters of ORYZA (v3) for Rice under Different Water and Nitrogen
954 Treatments and the Cross Treatments Validation, *Int J Agric Biol*, 20, 221-229,
955 2018.
- 956 Yan, Y., Ryu, Y., Li, B., Dechant, B., Zaheer, S. A., and Kang, M.: A multi-objective
957 optimization approach to simultaneously halve water consumption, CH₄, and
958 N₂O emissions while maintaining rice yield, *Agricultural and Forest*
959 *Meteorology*, 344, 109785, <https://doi.org/10.1016/j.agrformet.2023.109785>,
960 2024.
- 961 Yang, J. C. and Zhang, J. H.: Crop management techniques to enhance harvest index in
962 rice, *J Exp Bot*, 61, 3177-3189, 2010.
- 963 Yuan, S., Linqvist, B. A., Wilson, L. T., Cassman, K. G., Stuart, A. M., Pede, V., Miro,
964 B., Saito, K., Agustiani, N., Aristya, V. E., Krisnadi, L. Y., Zanon, A. J.,
965 Heinemann, A. B., Carracelas, G., Subash, N., Brahmanand, P. S., Li, T., Peng,
966 S., and Grassini, P.: Sustainable intensification for a larger global rice bowl,
967 *Nature Communications*, 12, 7163, [10.1038/s41467-021-27424-z](https://doi.org/10.1038/s41467-021-27424-z), 2021.
- 968 Zhang, B., Tian, H., Ren, W., Tao, B., Lu, C., Yang, J., Banger, K., and Pan, S.: Methane
969 emissions from global rice fields: Magnitude, spatiotemporal patterns, and
970 environmental controls, *Global Biogeochemical Cycles*, 30, 1246-1263,
971 <https://doi.org/10.1002/2016GB005381>, 2016.
- 972 Zhang, H., Zhang, S., Yang, J., Zhang, J., and Wang, Z.: Postanthesis Moderate Wetting
973 Drying Improves Both Quality and Quantity of Rice Yield, *Agronomy Journal*,
974 100, 726-734, <https://doi.org/10.2134/agronj2007.0169>, 2008.
- 975 Zhang, H., Adalibieke, W., Ba, W., Butterbach-Bahl, K., Yu, L., Cai, A., Fu, J., Yu, H.,
976 Zhang, W., Huang, W., Jian, Y., Jiang, W., Zhao, Z., Luo, J., Deng, J., and Zhou,
977 F.: Modeling denitrification nitrogen losses in China's rice fields based on
978 multiscale field-experiment constraints, *Global Change Biology*, 30, e17199,
979 <https://doi.org/10.1111/gcb.17199>, 2024.
- 980 Zhang, Y., Wang, W., Li, S., Zhu, K., Hua, X., Harrison, M. T., Liu, K., Yang, J., Liu,
981 L., and Chen, Y.: Integrated management approaches enabling sustainable rice
982 production under alternate wetting and drying irrigation, *Agr Water Manage*,
983 281, 108265, <https://doi.org/10.1016/j.agwat.2023.108265>, 2023.
- 984